Journal of Colloid and Interface Science 568 (2020) 234–244

Contents lists available at ScienceDirect

Journal of Colloid and Interface Science

journal homepage: www.elsevier.com/locate/jcis

Structure and swelling of cross-linked nanocellulose foams

Laila Hossain [a], Vikram Singh Raghuwanshi [a], Joanne Tanner [a], Chun-Ming Wu [b], Olga Kleinerman [c], Yachin Cohen [c], Gil Garnier [a,*]

[a] Bioresource Processing Research Institute of Australia (BioPRIA), Monash University, Clayton, Victoria 3800, Australia
[b] National Synchrotron Radiation Research Center, Hsinchu 30076, Taiwan
[c] Technion – Israel Institute of Technology, Haifa, Israel

GRAPHICAL ABSTRACT

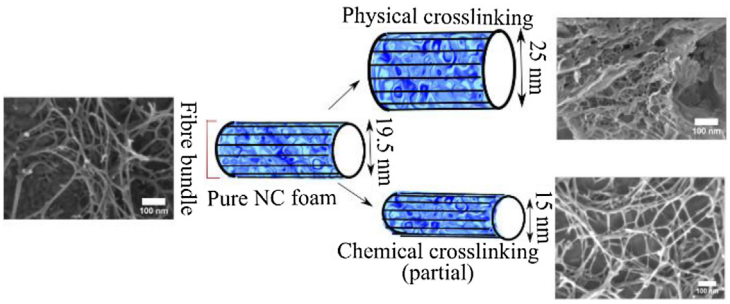

ARTICLE INFO

Article history:
Received 29 December 2019
Revised 12 February 2020
Accepted 13 February 2020
Available online 14 February 2020

Keywords:
Nanocellulose
Hydrogel
Foam
Crosslinking
Absorption capacity
Swelling
SAXS
SANS
FTIR

ABSTRACT

Hypothesis: The water absorption capacity of nanocellulose (NC) foam is tailored by crosslinking with polyethyleneimine (PEI) and hexamethylenediamine (HMDA). The interaction of amine groups in PEI and HMDA with the carboxylic groups (COO^-) of NC affects the foam structure which reduces its swelling capacity.

Experiments: Functionalised NC foams were prepared by TEMPO (2,2,6,6,-tetramethylpiperidine-1-oxyl) oxidation of bleached pulp, followed by fibrillation into a hydrogel, adding a crosslinker and freeze drying the hydrogel into a foam. The structure of the NC foam characterised by rheology, SANS (Small Angle Neutron Scattering), SAXS (Small Angle X-ray Scattering) and cryo-SEM (cryo-Scanning Electron Microscopy) was related to absorption and swelling properties.

Findings: The NC foam has the highest water absorption capacity at 132 g water/g foam. PEI-NC foam has a water absorption capacity of 71 g water/g foam, which further decreases to 47 g water/g foam for the HMDA-NC foam. Small angle scattering reveals the elementary fibril of NC is 3–5 nm thick and forms fiber bundles. In water, these bundles swell differently for the different types of foam which affects the water absorption capacity of the network. The structural analysis of the foam was related to the swelling capacity. The structure of NC foam can be engineered for specific applications for biomedical, agriculture or food industries.

1. Introduction

Hydrogels are hydrophilic physically or chemically crosslinked polymeric network materials which contain a large amount of water in their structure [1]. Hydrogels can be divided into two categories: biopolymer-based hydrogels and synthetic hydrogels-

* Corresponding author.
E-mail address: Gil.Garnier@Monash.edu (G. Garnier).

https://doi.org/10.1016/j.jcis.2020.02.048

depending on their source. Biopolymer based hydrogels have attracted particular attention because of their biocompatibility, biodegradability and high water absorption capacity [2].

Cellulose is the most abundant naturally occurring polymer and can be used to form hydrogels. Cellulose nanofibers, extracted from wood pulp through combinations of chemical and mechanical treatment, consist of semi-flexible fibrils [3]. Among the chemical methods, 2,2,6,6,-tetramethylpiperidine-1-oxyl (TEMPO) mediated oxidation is a widely known technique to introduce carboxylic groups (COO^-) to the fibre surface [4]. The electrostatic repulsion between the negative carboxylic groups facilitates the formation of a hydrogel upon mechanical treatment. There are many promising applications of these nanocellulose (NC) hydrogels in the biomedical, food and agriculture fields due to their large surface area, large water absorption capacity, sustainability and biocompatible characteristics [5].

Many crosslinking agents with cellulose based hydrogels have been investigated to achieve better mechanical property, control release of biological fluid and adsorption of specific particles. Epichlorohydrin, urea derivatives, aldehydes and aldehyde based reagents and carbodiimides are the most commonly used crosslinkers for cellulose based hydrogels [6]. Due to the toxicity and potential environmental hazard of these crosslinkers, research has targeted more suitable green crosslinker for NC. Chitosan, citric acid, succinic anhydride, polyethyleneimine (PEI) [7–11] have all been investigated to minimise potential hazards. PEI is a highly branched dendrimer of high cationic charge density [12,13] which attracts the negative COO^- group of oxidised fibres. As a non-hazardous polymer, PEI is used to physically crosslink the NC gel in this study. Hexamethylenediamine (HMDA) is used as a chemical crosslinker to compare the effect of chemical crosslinking in NC foam. In this study, NC foams are partially chemically crosslinked with HMDA to improve strength without important detrimental effect on absorption capacity of the foam.

NC foam can be produced by drying NC hydrogel. The resulting foam is highly porous (up to 99.7% porosity), of ultra-low density (10 mg/cm^3) [14,15] and can absorb water at more than 100 times its own dry weight. The absorption capacity depends on the chemical composition of the cellulose itself, as well as its surface area and pore size distribution, and the temperature, pH and ionic strength of the solution being absorbed [6,16]. The porosity and internal structure of NC foams largely dictate the absorption capacity and rate. This distinct structure of NC foams makes them unique compared to foam prepared from cellulose instead of NC. The absorption capacity can further be controlled by physical or chemical crosslinking the NC fibres. The higher the extent of crosslinking, the lower the absorption capacity due to compact structure [17,18]. Therefore, determination of the extent of structural change due to crosslinking is critical to the characterisation and understanding the mechanism behind the absorption capacity of NC foam.

Analysing NC foams upon swelling and de-swelling is particularly challenging, given their high water content and low solid content. A wide range of techniques have been used to characterise NC hydrogels [19] and dried foams; these include SEM and TGA [20], AFM [21], and SANS, SAXS and DLS [22]. Small Angle Scattering techniques, which enable representative analysis through the use of relatively large sample volumes, is emerging as an attractive NC foam characterisation method [19]. SAXS of TEMPO oxidised hydrogels was studied at different fibre concentrations to characterise the effect of fibre concentration. This was compared with the gel rheological properties to better understand the gelation mechanism [23]. Mao et al. used SAXS and SANS to characterise TEMPO oxidised homogenised cellulose nanofibers and the data were fitted using ribbon, parallelepiped and Gaussian-approximated parallelepiped models to calculate width and thickness of NC cross section [22]. In another study, microbial NC was studied dry and swollen to quantify the structure by a combination of Ultra SANS and SANS [24]. However, the effect of the fibrous network structure on the swelling capacity of NC-based foam was not explored, nor was the structure related to the swelling hysteresis in these studies.

It is the objective of this study to understand and quantify the relation between the structure and swelling behaviour of NC-based foams. It is clear that, although powerful and applicable, SAXS and SANS characterisation alone is insufficient to achieve this. In this study, a series of model physically and (partially) chemically crosslinked NC foams were saturated with H_2O/D_2O and measured using a combination of small angle scattering and cryogenic high resolution (HR) SEM techniques for the first time. Fibre swelling behaviour was measured and nano-scale structural changes related with changes in swelling capacities for different types of crosslinking were quantified. Thus, NC gel-foam properties have been directly related to and shown to control the absorption capacity of the foam via crosslinking. Attenuated total reflectance-Fourier transform infrared (ATR-FTIR) spectroscopy is performed to complement the cryogenic HR-SEM imaging technique and verify the effect of crosslinking on chemical composition and morphological structure. Comparison of crosslinked and non-crosslinked foam is presented to differentiate the structures and reveal the water transport mechanisms inside the structure. Insight into the mechanism of fibre bundle swelling on absorption capacity is also provided.

2. Methodology

2.1. Materials

Bleached Eucalyptus Kraft (BEK) pulp (approximately 10 wt% solids) was obtained from Australian Paper, Maryvale, Australia. 2,2,6,6-Tetramethylpiperidine-1-oxyl (TEMPO), Polyethyleneimine (PEI) of two different molecular weights (high molecular weight: $M_n \sim 60{,}000$; $M_w \sim 750{,}000$ and low molecular weight: $M_n \sim 600$; $M_w \sim 800$) and sodium bromide (NaBr) were purchased from Sigma-Aldrich. Hydrochloric acid (HCl) and Sodium Hydroxide (NaOH) were purchased from ACL Laboratories and Merck, respectively. HMDA was purchased from Chem-Supply. 12 w/v% Sodium Hypochlorite (NaClO) was purchased from Thermo Fisher Scientific and used as received. Milli-Q® water was collected from Merck Milli-Q® water purification system (Direct-Q® 3UV-R).

2.2. TEMPO mediated oxidation

The TEMPO-mediated oxidation process used in this investigation is based on a previously developed method [25]. There are two versions: the high charge and low charge methods, which yield 1.4 mmol and 0.6 mmol of carboxylate groups per gram dry weight of fibre, respectively. 25 g BEK pulp (dry weight) was suspended in 2500 mL water containing 0.4 g TEMPO and 2.5 g NaBr. In each case, a NaClO solution (12 w/v%) was initially adjusted to pH 10 by the addition of 32% HCl. To initiate the oxidation process, 100 mL NaClO (for high charge) or 75 mL NaClO (for low charge) were added drop-wise to the suspension whilst stirring. The pH of the reaction was monitored online and maintained at pH 10 by addition of 0.5 M NaOH. The oxidation process was completed in 3 h for the high charge (1.4 mmol/g) and 2 h for the low charge method (0.6 mmol/g). The oxidised fibres were recovered through filtration and stored refrigerated (2–8 °C). To produce hydrogel, TEMPO-oxidised pulp was dispersed in deionised water at a required concentration (0.5 wt% fibre concentration). Fibrillation is attained through a high-pressure homogeniser (GEA Niro Soavi

Homogeniser Panda) at 1000 bar for two passes. The oxidation process is critical to produce hydrogel as unoxidised fibre suspensions do not generate hydrogel. This hydrogel structure together with freeze drying process produces the porous foam structure.

2.3. Determining solids concentration

The solids concentration of all gels and pulps was determined through oven drying. The sample was weighed before (w_i) and after (w_d) drying. Sample moisture was removed by evaporation at 105 °C for at least 6 h. The solids content was calculated as:

$$Solid\ \ content(\%) = \frac{w_d}{w_i} \times 100\%$$

2.4. Conductometric titration

The carboxylate group (COO^-) content was measured by conductometric titration as reported in previous studies [26,27]. Approximately 30 mg (dry weight) of oxidised pulp was dispersed in 40 mL deionised water. 200 μL (1 wt%) NaCl was added to the dispersed sample. The pH of the sample was adjusted between 2.5 and 3 before titration with 0.5 M HCl. Titration was done by controlled addition of 0.1 M NaOH using a Mettler Toledo T5 titrator. The conductivity of the sample was monitored throughout the titration progress. The carboxyl group content (mmol COO^-/g fibre) was determined by using the following equation.

$$CC = \frac{c(V_2 - V_1)}{w} \times 1000$$

where V_1 and V_2 denote the amount of titrant required to neutralise the carboxylic groups (L), c is the NaOH concentration (mol/L), and w is the sample weight (g).

2.5. PEI incorporation

PEI was dissolved in deionised water at a concentration of 0.005 mg/mL. One-passed homogenised gel was mixed with PEI using a hand blender. Two different molecular weights of PEI (high molecular weight PEI: H_PEI = 750,000 Da and low molecular weight PEI: L_PEI = 800 Da) were used. The NC gel was mixed with PEI at a mass ratios of 1: 0.07 (NC:PEI). The resulting mixture was then passed through the homogeniser again. All the passes through the homogeniser were performed at 1000 bar. PEI at lower concentration (NC:PEI = 1:0.05) was also studied with NC which showed similar swelling behaviour but lower gel strength compared to NC:PEI = 1:0.07. Only NC:PEI = 1:0.07 sample was considered for this study as it increased the mechanical property (strength) of the gel compared to pure NC gel.

2.6. HMDA incorporation

HMDA was dissolved in deionised water at a concentration of 0.45 mg/mL. The NC gel was mixed with the HMDA solution at stoichiometric ratios of 1:4 and 1:8 (COO^-:NH_2). HMDA does not react with NC at room temperature or below room temperature if no reagent (such as EDC/NHS) is used to activate the COO^- group in NC. So, the resulting mixture was cured at 80 °C for 1 h in an oven. The final cross-linked gel was removed and stored at 4 °C. The molecular structure of PEI and HMDA is shown in Fig. 1.

2.7. Gel rheology measurement

Rheological testing was performed with an Anton Paar MCR302 rheometer at 25 °C. A cone (0.997°) and plate (49.975 mm) geometry were selected. A solvent trap was used to make sure steady temperature during measurements. Amplitude sweep was done from 0.01 to 100% at a constant frequency of 1 Hz.

2.8. High-resolution scanning electron microscopy (HR-SEM)

Gel morphologies were imaged by high-resolution scanning electron microscopy (HR-SEM) using cryogenic sample preparation method. Sample preparation was carried out in a controlled-environment vitrification system (CEVS) [28], followed by complete sublimation of vitrified water. Approximately 3 μL of gel was placed between two gold planchettes, and the "sandwiched" gel vitrified by rapid immersion in liquid nitrogen. The vitrified sample was loaded on a specimen holder, which was subsequently transferred under cryogenic conditions into the pumped BAF060 freeze-fracture replication system (Leica, Vienna), the stage of which was pre-cooled to −160 °C. In the BAF060 unit, the sample was fractured and stabilized until the vacuum reached 10^{-6} mBar, maintaining the temperature around −160 °C. To remove the water phase, the temperature of the sample was raised to −100 °C, at which water has a vapor pressure of about 10^{-5} mBar. The sample was maintained at this temperature for two hours to ensure complete water sublimation. This combination of the high vacuum and low temperature provides ideal conditions to achieve water removal and preserve the mechanical strength of the frozen gel. Subsequently, the liquid nitrogen flow was turned off, and the sample kept inside the BAF060 under vacuum until ambient temperature was reached. This final slow temperature ramp mitigates collapse of the gel structure. The freeze-dried sample was transferred directly to the SEM in the sample holder via the cryogenic port of the microscope (Leica, Vienna). Unlike classical freeze-drying procedures, no shadowing or conductive coating was applied to the sample. Imaging was performed by a Zeiss Ultra Plus high-resolution scanning electron microscope equipped with a Schottky field-emission electron gun and a unique Gemini electron-beam column design (Carl Zeiss SMT GmbH Oberkochen, Germany). To achieve high-resolution images close to the isoelectric (no-charging) point, the microscope was operated at 1 kV electron beam energy. Images were acquired by mixing signals from a classical Evart-Thornley and a high-resolution In-the-Lens secondary electron (SE) detectors, at working distance of about 3.5 mm.

2.9. Fourier transform infrared (FTIR) spectroscopy

The crosslinked foams were tested by ATR-FTIR using the Agilent Cary 630 FTIR Spectrometer. The freeze dried foams were tested for the FTIR spectra to determine the type of crosslinking.

2.10. Preparation of NC foams

To prepare the foams, 15 g of gel was spread evenly onto a 55 mm petri dish. The sample was frozen at −80 °C, then freeze-dried (Christ Alpha 2–4 LD Plus) for 2 days. The freeze-dried samples (pure nanocellulose foam: NC foam, nanocellulose crosslinked with high molecular weight PEI: NC_H_PEI foam and nanocellulose crosslinked with HMDA having stoichiometric ratio of 1:8 for COO^-:NH_2 = NC_HMDA_18 foam) are shown in Fig. 2.

2.11. Free swell capacity

15 g of gel sample was freeze-dried in a 55 mm petri dish to produce a NC foam which was tested for free swell capacity. The sample was deposited in a funnel (funnel filter glass, 75 mm diameter) and placed in a beaker full of Milli Q® water. The water absorbed was measured at regular intervals up to 3 h. Before measuring the weight of water absorbed, the funnel with the sample

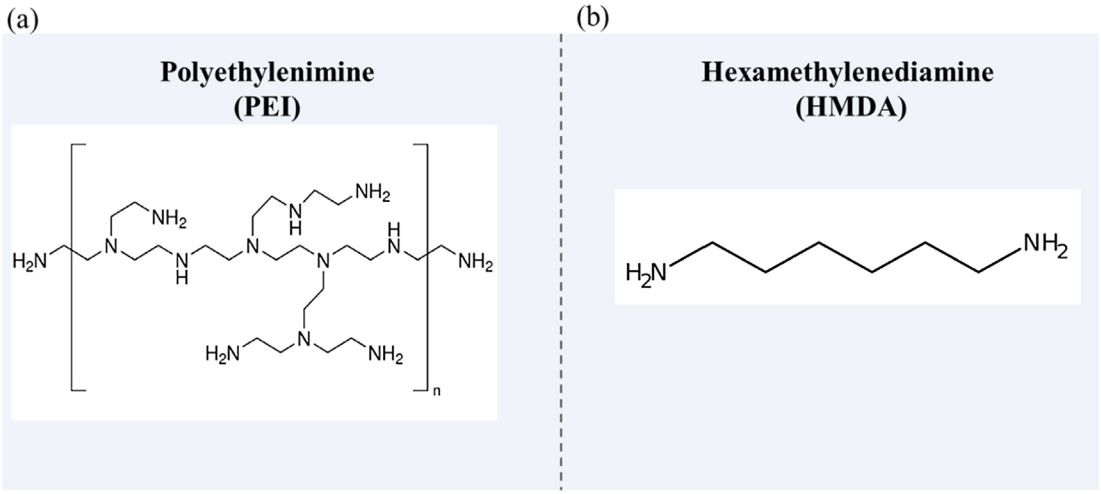

Fig. 1. Molecular structures of the crosslinking agents: (a) PEI and (b) HMDA.

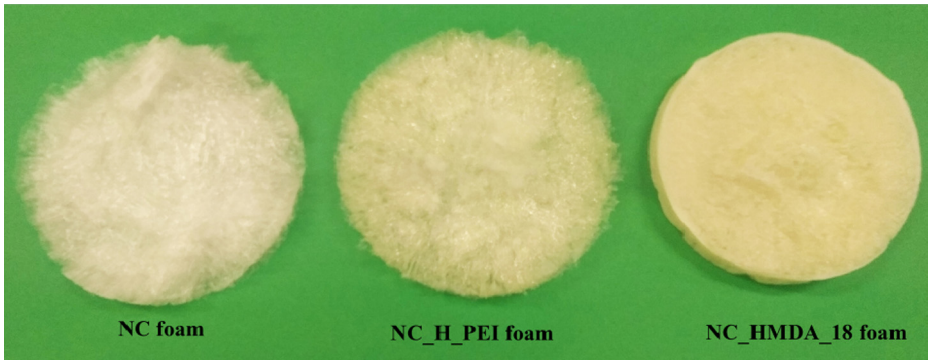

Fig. 2. Picture of the three types of foams: NC foam, and NC foam crosslinked with high molecular weight PEI and HMDA, respectively.

was removed from the fluid container and kept on an inclined surface for five minutes for the excess liquid drip off.

The free swell capacity was then calculated as follows:

$$\text{Free Swell Capacity (FSC)} = \frac{m_t - m_i}{m_i}$$

where m_t is the mass of the swollen foam at a particular time interval and m_i is the initial mass of the foam.

2.12. Small angle neutron and small angle X-ray scattering

Small-angle neutron scattering (SANS) measurements were performed at the Time-of-Flight BILBY beamline at the Australian Nuclear Science and Technology Organisation (ANSTO), NSW, Australia. The wavelength of 6 Å was conducted by using its neutron-velocity selector (NVS). Two detector carriage lengths were used to cover the Q-range from 0.00254 to 0.31 $Å^{-1}$. The foam samples were placed in demountable cells of wall thickness 2 mm. D_2O was used to hydrate the samples.

The data collected were reduced by using the Mantid software with the BILBY package. The background of the empty cell was subtracted from each sample measured without D_2O, and the D_2O scattering was subtracted from the hydrated samples. The raw data was normalised to the absolute scattering values by the pre-calibrated scattering curve of D_2O.

Small angle X-ray Scattering (SAXS) was performed at the SAXS/WAXS beamline of the Australian Synchrotron [29]. The foam was measured in-situ during dehydration. SAXS measurements were made at an energy of 12 keV (λ = 1.033 Å) at a sample to detector distance of 7 m (q range:0.001 and 0.1 $Å^{-1}$). The scattered photons were collected using a PILATUS 1 M detector (pixel size 172 μm × 172 μm). Q scale was calibrated using the standard silver behenate. Data reduction and radial averaging of scattering curves was performed by the beamline specific Scatter Brain software.

3. Results

The free swell capacity of NC foam and crosslinked NC foams is tested by immersion into MilliQ® water. The free swell capacity of the foam is related to the morphological and internal structure, which are determined by HR-SEM and small angle scattering (X-rays and neutrons). The foam internal structure is quantified by network stiffness, swollen bundle diameter and structure compactness to determine the effect of crosslinking on the foam structure. Hydration-dehydration study are also performed to estimate the effect of dehydration/drying time on nanostructure.

3.1. Swelling behaviour of NC foams

Swelling is tested by immersing the NC foams in MilliQ® water. Fig. 3 shows the free swell capacity (in g water/g foam) for the pure NC, NC_PEI and the NC_HMDA_18 foams. The free swell capacity for the pure NC foam is 132 g water/g foam. Foams from PEI and HDMA treated NC have a reduced free swell capacity of 71 g water/g foam and 47 g water/g foam, respectively.

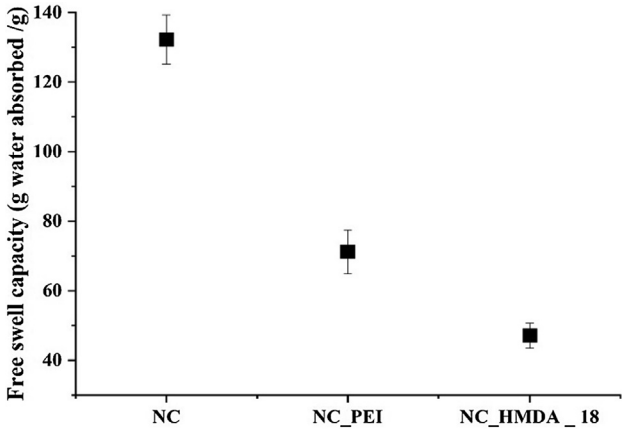

Fig. 3. Comparison of the free swelling capacity for the different NC foams.

3.2. Morphological structure

High-resolution scanning electron microscopy (HR-SEM) is performed on gel samples prepared by the cryogenic method to evaluate the morphology of the pure NC, NC_PEI and NC_HMDA gels. All gels show highly crosslinked and reticulated structures with low fibrous solid content, as expected.

The HR-SEM micrographs of NC (Fig. 4a) and NC_HMDA gels (Fig. 4c) show the distribution of cellulose fibres (of diameter 10–30 nm) creating porous structures with large pores of diameter ranging from 50 to 200 nm.

The HR-SEM micrograph of the NC_PEI gel presents a different morphological structure and fibre distribution (Fig. 4b). The NC_PEI gel has a flake-like and fluffy structure.

3.3. FTIR spectra of modified NC foams

Freeze dried NC, NC_PEI and NC_HMDA foams are analysed by ATR-FTIR. Fig. 5a compares the ATR-FTIR spectra of NC and NC_PEI foams. Both spectra are similar in shape, indicating that PEI induces no significant chemical change to the NC foam chemical bonding.

Fig. 5b shows the spectra of NC and NC_HMDA foams. The NC spectra display the representative COO^- group peak at 1599 cm^{-1} corresponding to the C=O stretch. The C=O stretch peak shifts to a broader peak in the amide crosslinked foam (NC_HMDA) at 1589 cm^{-1}. As this was partial crosslinking, the C=O stretch is not very prominent. FTIR spectra for complete crosslinking of NC with HMDA is provided in Fig. S1 of the supplementary information section.

3.4. Rheological properties of crosslinked gel

The viscoelastic behaviour of the NC gel and, NC_PEI and NC_HMDA crosslinked gels, is quantified by rheology (Fig. 6). The Elastic (G′) and Viscous (G″) moduli of the 3 gels were measured in oscillatory flow mode as a function of shear strain. There are four observations of interest. The first is that the rheology of all three gels is dominated by the elastic regime: G′ remains higher than G″ over most of the strain range. The second is that all three gels have a clear and fairly similar linear viscosity region (LVR) that drops at a strain of 10%. The strain at which the LVR regime drops is a little higher for NC_HMDA gels, indicating stronger cohesion between the NC fibres. The third observation is that PEI increases the elastic modulus of NC gels (G') by a factor of 5 compared to the NC gel, while HMDA provides no increase; increase in G' gives an indication of the relative crosslinking densities. Fourth, the slope of the elastic curve (G') after linear viscoelastic region (LVR) for NC_HMDA_18 and NC_H_PEI became steeper compared to NC gel which is also showing some gel crosslinking. The crosslinking densities of these samples calculated from the elastic moduli are provided in Table S2.

3.5. Structural change of foam upon swelling

NC foams are characterised in the dried and hydrated states by Small Angle Neutron (SANS) and X-ray (SAXS) Scattering. SANS and SAXS are both non-destructive methods that provide average structural information of nanomaterials using a relatively large sample volume compared to other techniques [30,31].

Fig. 7a shows the SANS curves for NC foams made from fibres of two different charges (*HSC*: 1.4 mmol COO^-/g fibre and *LSC*: 0.6 mmol COO^-/g fibre). In the dried state, both materials show

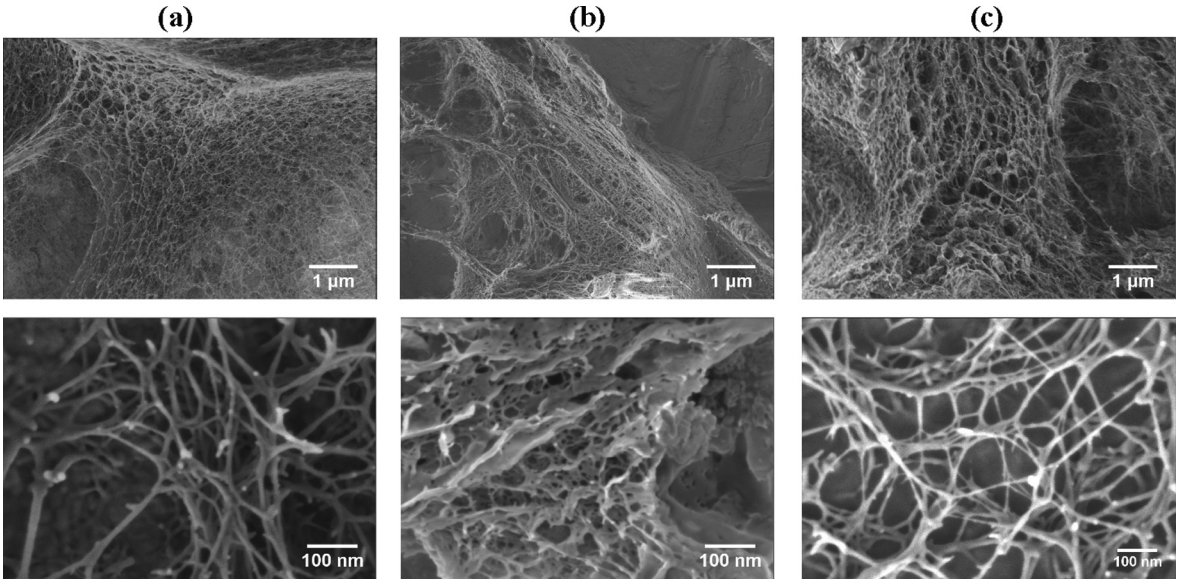

Fig. 4. HR-SEM images of (a) 0.5 NC gel, (b) NC_ H_PEI (NC:H_PEI = 1:0.125) gel and (c) NC_HMDA_12 gel at complementary magnifications.

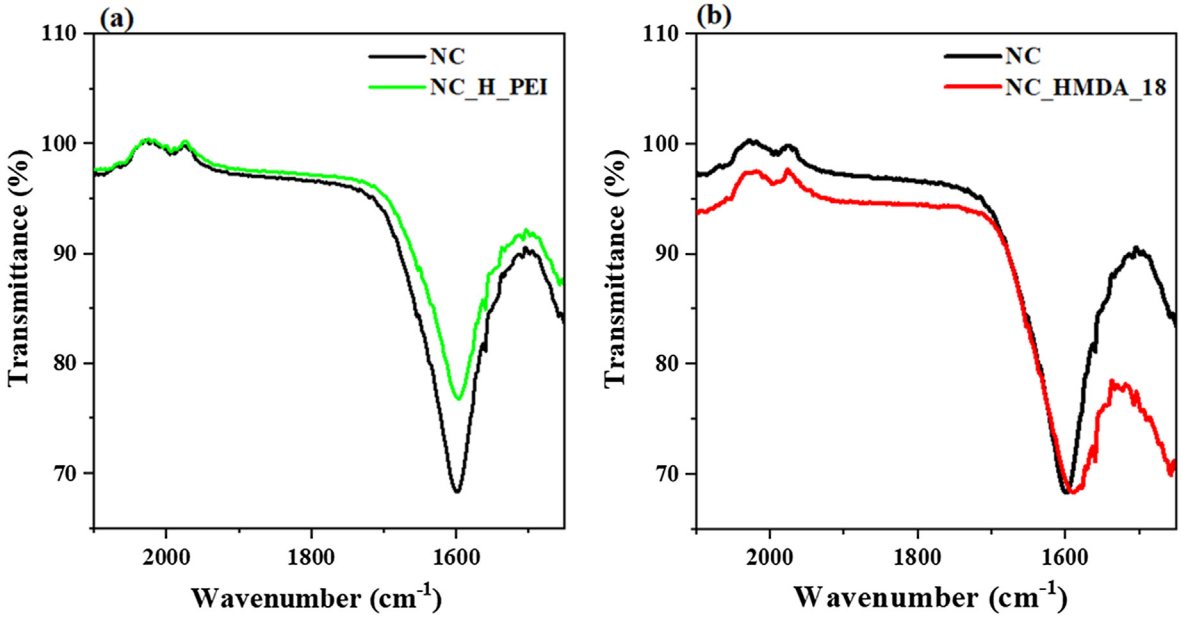

Fig. 5. ATR-FTIR spectra for (a) pure NC and NC_H_PEI foam, (b) pure NC and NC_HMDA_18 foam.

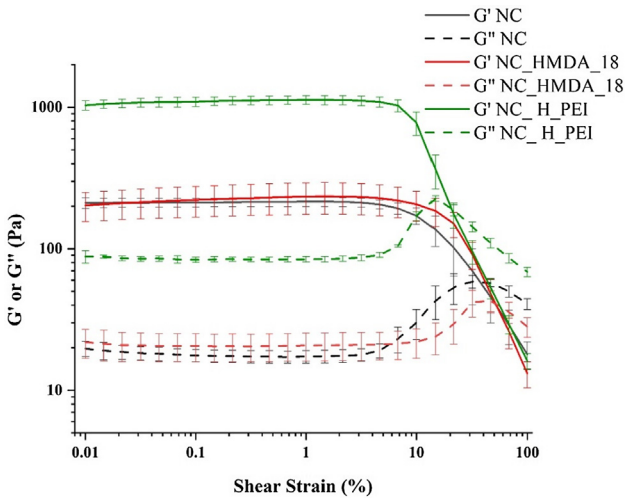

Fig. 6. Rheological spectra of pure NC, NC_H_PEI and NC_HMDA_18 hydrogel: dynamic strain sweep (25 °C) at a frequency of 1 Hz.

the same scattering profile with no evidence of organised structure. The slope of the scattering curve ($q < 0.02$ Å^{-1}) displays q^{-4} power law behaviour, which indicates scattering from large size aggregated fibres. NC fibre charge density did not affect the gel network structure.

Upon hydrating the sample with D_2O, a significant hump appears in SANS profile (Fig. 7a) in the q range of 0.02–0.1 Å^{-1}. This hump corresponds to a change in the structure in the size range 1–30 nm. Both HSC and LSC samples show the same structure scattering profile, indicating that the charge of the cellulose fibres has no effect on the structure upon hydration of the freeze-dried foam. The upturn in the data at low q values ($q < 0.02$ Å^{-1}) in the hydrated SANS curves indicates inhomogeneity of the large-scale structures.

Fig. 7b shows the SANS curve for the NC foams made with PEI of different molecular weights (750,000 Da and 800 Da). No structure change is observed for the freeze-dried samples. However, upon hydration, a minor change in slope can be seen (Fig. 7b) which is attributed to the change in PEI molecular weight.

The SANS curves of the NC_HMDA foams show noticeable changes in the scattering curve intensity upon hydration and for freeze dried condition. (Fig. 7c). However, the structures of the scattering curve profile are identical. The freeze-dried NC_HMDA_18 shows higher scattering than the NC_HMDA_14 foam. Upon hydration with D_2O, the NC_HMDA_14 foam absorbs more water and shows higher scattering intensity compared to NC_HMDA_18.

3.6. Probing fibrous structure by different models

The structural information from the scattering curves are extracted by fitting with three different models. These are: (i) the flexible elliptical cylinder model with the power law [32]; (ii) the mass fractals model with power law [33] and (iii) the Debye-Bueche and Lorentzian function [34]. The first model calculates the cross section and the diameter of the fibre with the stiffness of the network structure in terms of persistence length. The second model characterises the mass fractal distribution in the hydrated foam structures. The third model quantifies the large and small correlation lengths. Detailed model description is provided in supplementary information S3.

The scattering data is fitted by the flexible ellipsoidal cylinder model to quantify the elementary fibril dimension. This model considers ellipsoidal cross-sectional rods defined by the cross-section minor radius r_a, the axis ratio r_b/r_a, the persistence length (l_p) and the contour length (L) [35]. The Kuhn length, which is a measure of stiffness, is twice the persistence length [23]. The contour length represents the length of the chain [36].

Fitting all samples (q range: 0.01–0.2 Å^{-1}) with the flexible elliptical cylinder model yields average cross-sectional fibre dimensions of 3 nm × 5 nm using an assumed contour length of 1000 nm [35]. The current results complement a previous study on TEMPO oxidised homogenised cellulose nanofiber which showed that the width and thickness of the cross section are 2 nm and 8 nm, respectively [22].

The persistence length (network stiffness) evaluated with the flexible cylinder model is shown in Fig. 8a. For the pure NC foam, the persistence length is 9 nm and increases to 12 nm for NC_H_

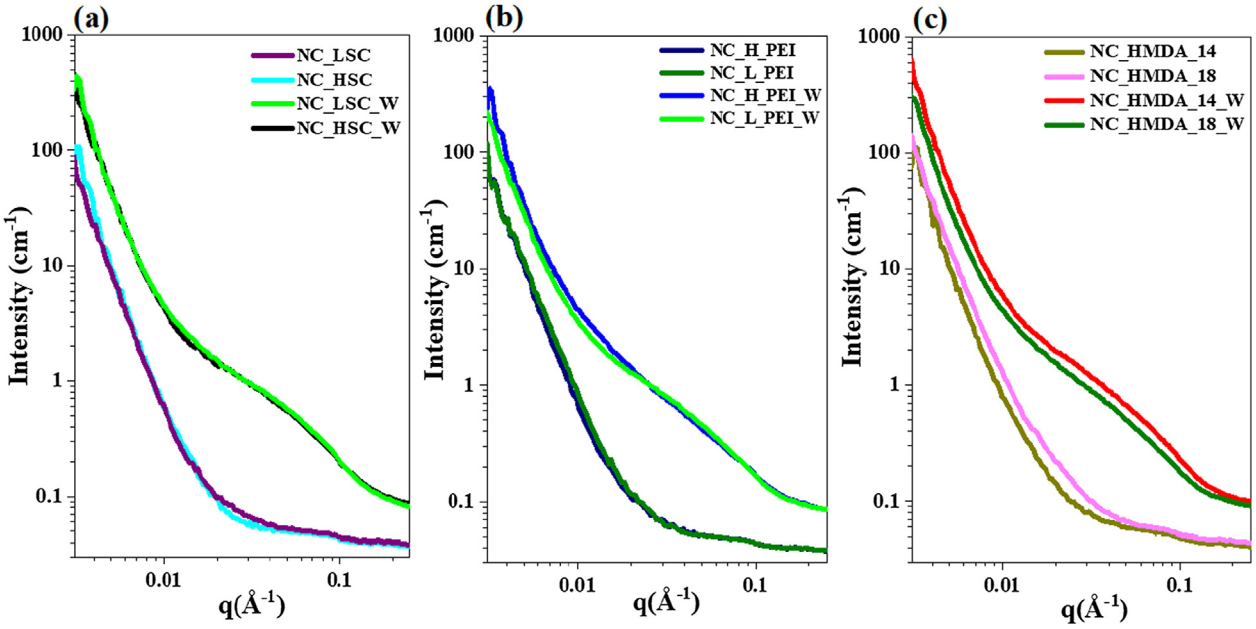

Fig. 7. SANS intensity-q relationships for dry and saturated (w denotes water saturated foam) foams with hump made from NC gels original, NC_H_PEI and NC_HMDA. (a) Effect of surface charge, (b) physical crosslinking and (c) chemical crosslinking on the foam.

PEI foam. The NC_HMDA foam indicating that partial chemical crosslinking results in a higher persistence length.

Fitting the SANS data with the mass fractal model combined with the power law q^{-4} (q range 0.004–0.2 Å^{-1}) reveals the cut-off length (Fig. 8b) to be equivalent to the swollen fibre bundle dimension, which is between 12 and 26 nm. The NC_H_PEI foam swells more than NC_L_PEI indicating that increasing the molecular weight of PEI increases fibre bundle swelling. However, the NC_HMDA foam did not swell much and the bundle size reduced to 14 nm. The NC_HMDA_14 foam has its fibre bundles swelling to 17 nm, which decreased to 14 nm upon increasing the HMDA concentration (1:8) for NC_HMDA_18 foam.

The calculated mass fractal dimensions reveal the compactness/openness of the network structure (Fig. 8c). The pure NC foam has a fractal dimension of 1.2. Adding the low molecular weight PEI (NC_L_PEI) does not change the dimension significantly, and the high molecular weight PEI (NC_H_PEI) provides foams with a mass fractal dimension of 1.1. The NC_HMDA_14 and NC_HMDA_18 foam show increase in mass fractal dimensions to 1.3 and 1.4, respectively, for foams at the low and high HMDA ratio. The low values of the fractal dimensions indicate the openness of the structure. However, the differences in the fitted values may not be significant and other factors in structure heterogeneities may contribute to differences in fractal dimensions calculated via the mass fractal analytical method.

The correlation length evaluated by the Debye-Bueche and Lorentzian function indicates the large and small scale heterogeneities in the swollen fibre bundles and in the network. The smaller correlation length of 3–5 nm represents the dimensions of the elementary fibril unit. The higher correlation length (Fig. 8d) was obtained between the size range of 70–90 nm. These concentration fluctuations occur due to the distributions of the large cellulose fibres bundle size or pore size. The highest correlation length was found for the H-PEI NC foam, which indicates a loose structure. For pure NC foam, the correlation length was 79 nm resulting from the big pores or large size fibre bundles. For the NC-HMDA foam, the correlation lengths decreased as HMDA concentration increased.

3.7. NC foam hydration and dehydration behaviour

SAXS experiments were performed at the SAXS/WAXS beamline of the Australian Synchrotron to evaluate the hydration and drying behaviour of NC foam. The freeze-dried foam was hydrated with MilliQ® water. Fig. 9 compares the SAXS curves of the original freeze dried NC foam structure (designated as blank) to the hydrated NC foams after 10, 13 and 15 min during drying under ambient conditions (Fig. 9).

A sharp hump is observed at saturated condition in the q range between 0.03 and 2 Å^{-1}. The sharp hump started decaying with time and after 15 min, the hump completely disappeared. But the profile of freeze-dried foam (blank in Fig. 9a) and the once saturated dried foam (15 min in Fig. 9a) is different. This indicates that the foam does not return to its original structure after drying from saturated condition.

All foams show an asymptotic decay of q^{-4} at low q region ($q < 0.03$ Å^{-1}), originating from a smooth interface of fibre bundle (Fig. 9a). The scattering curves were fitted with the mass fractal combined with the power law model, which calculates the cut-off length and the mass fractal dimensions (Fig. 9b).

The saturated NC foam shows a cut-off length (swollen fibre bundle diameter) of 19 nm and a mass fractal dimension of 1 (Fig. 9b). Upon ambient drying, the cut-off length decreased to 14 nm, indicating the removal of water from the structure, which increases the compactness or shrinkage of the NC fibre bundle. The mass fractal dimension increased to 2.6 which complements the cut-off length results.

4. Discussion

The swelling behaviour of freeze-dried NC foam crosslinked with PEI (physically) and HMDA (partially chemically) was studied and related to water absorption. The measured free swell capacity of NC foam (132 g water/g foam) indicates that the pure NC foam has a higher absorption capacity than the PEI (65 g water/g foam) and HMDA (48 g water/g foam) crosslinked NC foams (Fig. 3). This

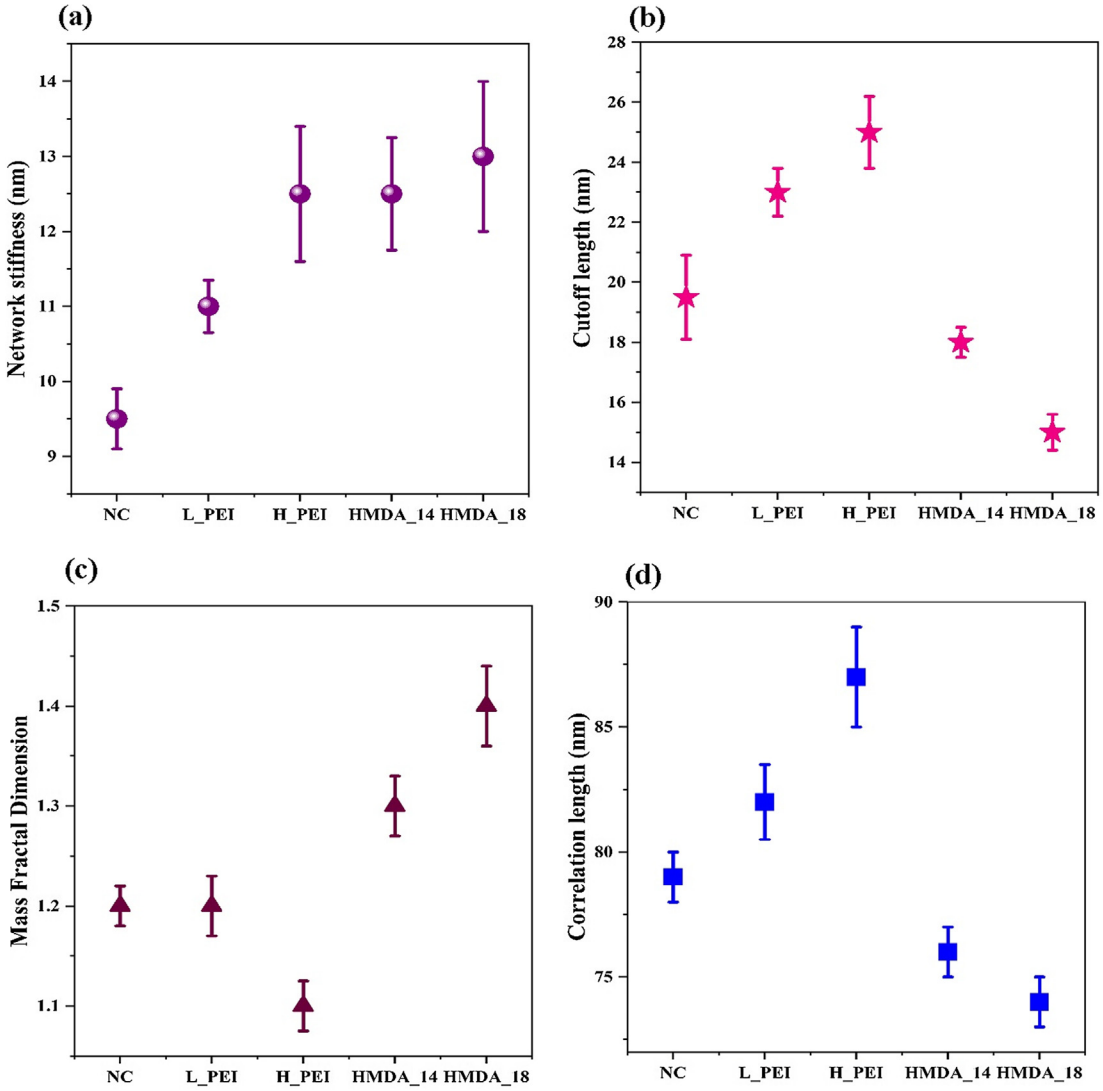

Fig. 8. Structural characterisation of swollen NC foam based on SANS data: (a) network stiffness, (b) cut-off length, (c) mass fractal dimension and (d) correlation length. (L_PEI = NC with 7% LMW PEI; H_PEI = NC with 7% HMW PEI; HMDA_14: NC with HMDA and COO^- : NH_2 = 1:4; HMDA_18: NC with HMDA and COO^- : NH_2 = 1:8).

is attributed to a combination of two mechanisms directly related to crosslinking: (i) differences in the physical structure of the foams and (ii) screening of some of the native carboxyl groups on the NC fibres. The zeta potential of selected samples is shown in Table S4 of the supplementary information section. NC foam is composed of entangled, TEMPO oxidised homogenised cellulose nanofiber bundles. The TEMPO reaction oxidises the secondary OH of the C6 carbon of cellulose into a carboxyl (COO^-) group. The pure NC foam has a carboxylic concentration of 1.4 mmol COO^-/g fibre. The negatively charged carboxyl groups interacts with water molecules which increases water absorption capacity of the NC fibre structure [27].

The fibre bundles of NC foam structure are made of elementary fibrils (elementary fibril shown in Fig. 10) units of cross section 3 nm × 5 nm as determined by fitting the SANS curves with the flexible elliptical cylinder model. When the NC foam is soaked in water, the liquid diffuses by capillary flow between the elementary fibrils and interferes with the carboxyl groups (H bonding) resulting in swelling of fibre bundles (Fig. 10). NC foam fibre bundles swell up to 19.5 nm, which is larger than the NC_HMDA foam (15 nm) but smaller than the NC_PEI foam (25 nm).

The NC_PEI foam fibre bundles swell more (25 nm) at the nanoscale but this type of foam absorbs less water (65 g absorbed/g foam) at the macroscale compared to the pure NC foam (132 g water/g foam). During homogenisation of PEI with NC fibre, the big molecules of PEI (M_W = 750,000 Da) may diffuse into the fibre bundle, expanding the bundle structure (Fig. 10) and establishing some physically crosslinking with carboxyl groups. This hypothesis of a more open structure is corroborated by the mass fractal dimension of 1.1 (calculated from the SANS curves fitting) which indicates that the NC_PEI structure is less compact than that of pure NC foam. The cryogenic HR-SEM micrographs complement the SANS analysis showing the open flake like structure of the NC_PEI foam (Fig. 4). The PEI crosslinked NC fibre shows a high network stiffness with a persistence length of 12.8 nm (Fig. 8a) which is higher than that for the pure NC foam (9 nm). Higher network stiffness upon crosslinking is also shown by the rheology results (Fig. 6), as the slope of the PEI crosslinked gel is steeper than for the pure NC gel.

Upon contact with water, the water molecules diffuse into the NC_PEI fibre bundles and through the pores formed by the network of crosslinked fibre bundles. The open and fluffy structure of

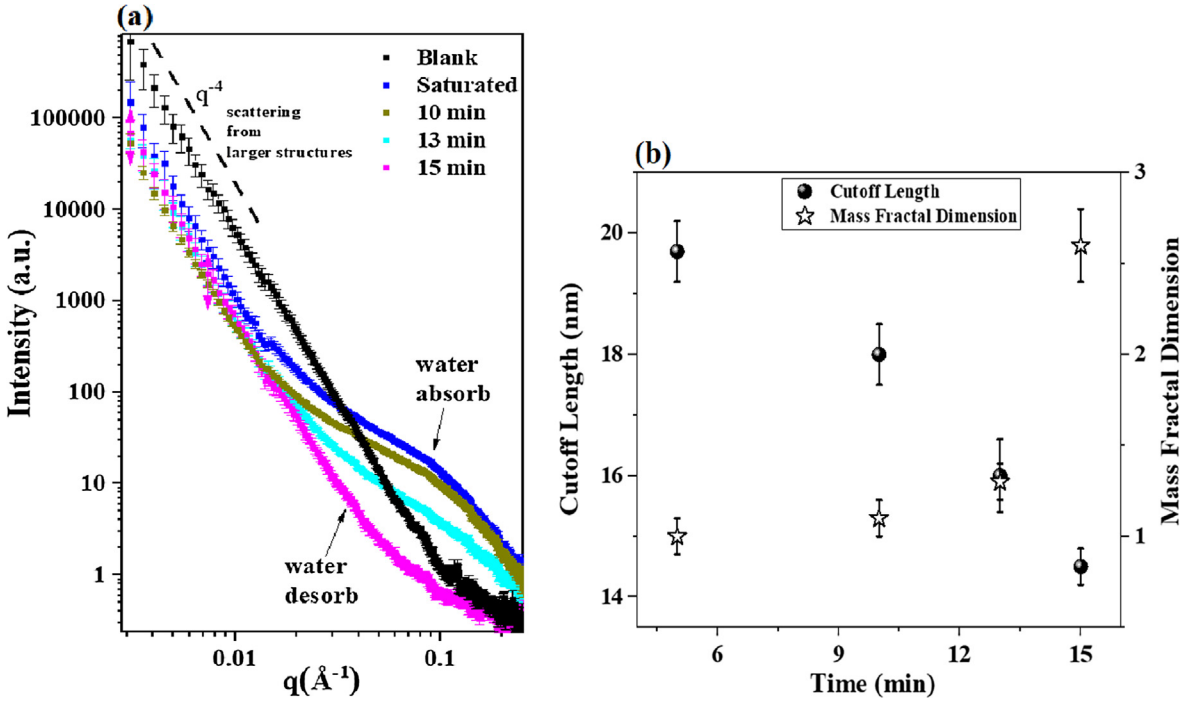

Fig. 9. Structural change of NC foam upon swelling and deswelling in SAXS: (a) SAXS intensity-q relationships for NC foam (Blank is dry sample and others are after X min of saturation in water where X = saturated, 10, 13 and 15 min) and (b) cutoff length and mass fractal dimension for NC foam.

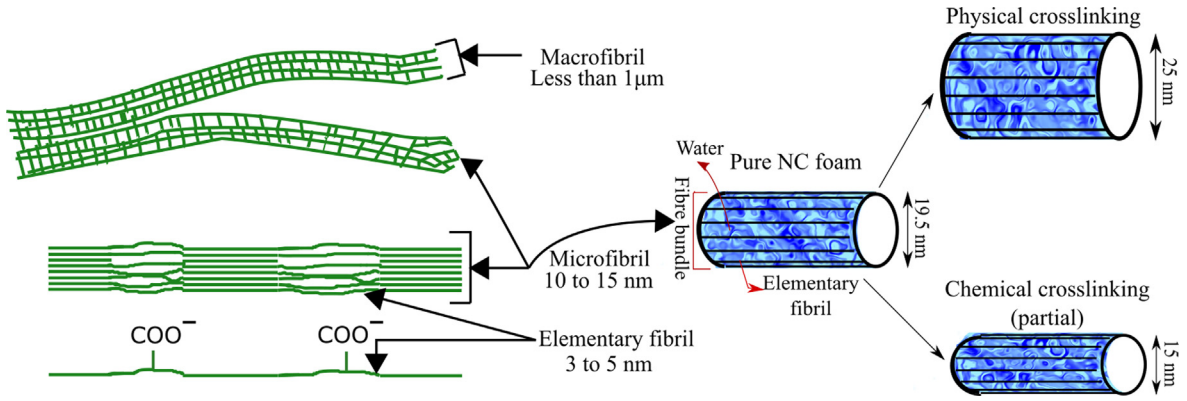

Fig. 10. Schematic diagram showing the length scale of the NC gel. A flexible ellipsoidal cylinder model was selected to measure the effect of PEI (physical crosslinking) and HMDA (partial chemical crosslinking) on the NC fibre bundle swelling.

NC_PEI foam accommodates most of the water in the network, resulting in higher fibre bundle swelling.

However, at the macroscale, the lower water absorption capacity of NC_PEI (Fig. 3) results from the open and stiff fibrous network in this sample, combined with screening of some of the COO^- groups by the primary, secondary and tertiary amine groups of the adsorbed PEI molecules (Fig. 1).

In contrast, in NC_HMDA foam, the HMDA molecules can diffuse into the NC fibre bundle. Due to the smaller size of the HMDA molecule (M_W HMDA = 116.2 Da) and their interaction with the COO^- groups in the fibre bundle, the resultant NC_HMDA fibre bundle structure is more tightly bound together, and therefore it shrinks [37]. The NC_HMDA foam thus has a more compact fibrous network than the pure NC and NC_PEI foams (Fig. 8c and Fig. 10) as shown by the calculated NC_HMDA_18 mass fractal dimension of 1.4. The compactness of the foam structure increased with the HMDA concentration, as shown by the mass fractal results (Fig. 8c) which increases the extent of crosslinking.

NC_HMDA foam showed the lowest swelling capacity (48 g water/g foam). This is due to the compactness of fibre bundle which restricts and hinders the water diffusion and penetration in the fibre bundle structure. The tighter structure also reduces the swelling of the fibre bundle to 15 nm. Another reason which contributes to the reduction of water absorption capacity is the screening of some COO^- groups by the two primary amine groups from each molecule of HMDA.

The SAXS hydration-drying study quantifies the structure compactness upon swelling and deswelling. For the dry foam, SAXS shows a power law behaviour which indicates scattering from the surface of aggregated fibres. During swelling, the fibre bundles and pores accommodate water. The water penetrates into the fibre bundle and the inter-elementary fibril distance increases which opens the fibre bundle. This is seen by the low mass fractal (1.0) value after saturation. Upon drying, the water from the bundles evaporates and the inter-elementary fibril distance decreases, as structure shrinks, and the elementary fibrils aggregate inside the

bundle. This leads to an increase in the compactness of the internal structure of the bundles as revealed by the increased mass fractal dimension (2.5).

Interestingly, the freeze-dried foam structure differs from the dehydrated sample (Fig. 9). The fibre bundle dimension, represented by the cut-off length, decreased from 19 nm to 14 nm upon hydration and subsequent ambient drying. The swollen hydrated fibre bundle has higher cut-off length and upon drying, the water evaporates and the fibre bundle shrinks to their decreased cut-off length 14 nm. This increased compactness is attributed to the formation of aggregates during room temperature drying. Freeze drying sublimation occurs at temperature ranging from −20 °C to −50 °C, at a lower pressure than for the triple point of water, to deliberatively minimise the aggregation of cellulose fibres [38]. However, during ambient drying, the NC fibres have the ability to migrate, resulting in aggregation as water evaporates [39].

The combined effect of physical entrapment and COO^- groups give pure NC foam a higher water absorption capacity than PEI/HMDA modified foams. In contrast, network stiffness increases with PEI and HMDA crosslinking. Therefore, NC foam structure and swelling capacity can be controlled by crosslinking the fibre structure using PEI and HMDA of varying molecular weights and concentrations.

5. Conclusion

This study relates the NC gel-foam properties to their structure controlled by physical and partial chemical crosslinking. The structure and swelling behaviour of freeze-dried NC foams based on TEMPO oxidised NC gels were investigated. NC gels were crosslinked physically and chemically (partially) by the addition of PEI and HMDA, respectively. The gels were characterised by rheology to assess the level of crosslinking and by HR-SEM for morphology evaluation. The chemical composition of the foams was analysed by FTIR, and their water absorption capacity was determined. SANS and SAXS analysis were performed on the dried foams and saturated foams at different levels of drying.

Functionalised NC foam networks can absorb up to 132 times their own weight in liquid. Water diffusion inside the cellulose nanofibrils swells the constitutive fibre bundle up to 19.5 nm. NC-PEI crosslinking expands the foam structure, which results in higher fibre bundle swelling at the nanoscale (25 nm), but lower absorption capacity at the macroscale (71 g/g) compared to the pure NC foam. In contrast, NC-HMDA crosslinking creates a more compact foam. The NC-HDMA fibre bundle swelling was only 15 nm due to the restriction of migration of water into the more compact fibrous network.

The hydration-dehydration behaviour of NC foam shows the change of fibre bundle diameter during drying, confirming fibre bundle shrinkage from 19 nm to 14 nm upon drying. As drying progresses, the fibre bundle structure becomes more and more compact. After drying (air drying), the fibre bundle structure does not return to its original freeze-dried NC foam structure because of the different drying method.

Carboxylated nanocellulose foams have been prepared as superabsorbent in a previous study [27]. Crosslinking NC foams with PEI and HMDA can be used as a method to control and tailor the swelling capacity of NC foams. Cellulose nanofibre structure has been studied in dry and aqueous suspension [15,40]. However, previous studies did not explore the structural change of crosslinked NC foams nor the mechanism of hydration-dehydration. In this study, structural change was analysed in the context of swelling upon water absorption for crosslinked foam. Relating the fibre swelling capacity to the internal fibrous structure of a NC foam allows to engineer this material for specific and targeted food, agriculture, personal care and biomedical applications.

CRediT authorship contribution statement

Laila Hossain: Prepared samples, conducted all experiments and wrote manuscript. **Vikram Singh Raghuwanshi**: Performed SAXS and SANS experiments, data analysis and wrote manuscript. **Joanne Tanner**: Data analysis and wrote manuscript. **Chun-Ming Wu**: Performed SANS experiments. **Olga Kleinerman**: Performed cryo-SEM experiments. **Yachin Cohen**: Performed cryo-SEM experiments, data analysis and wrote manuscript. **Gil Garnier**: Performed data analysis and wrote manuscript.

Declaration of Competing Interest

The authors declare that they have no known competing financial interests or personal relationships that could have appeared to influence the work reported in this paper.

Acknowledgements

This work was supported by Food and Dairy Graduate Research Industry Partnership, Victorian Government, Monash University and Meat and Livestock Australia (MLA). The authors acknowledge the SAXS/WAXS beamline at the Australian Synchroton and BILBY SANS beamline at the Australian Nuclear Science and Technology Organisation (ANSTO). Electron microscopy preparations and imaging were done at the Technion Center for Electron Microscopy of Soft Matter, and we acknowledge Prof. Yeshayahu (Ishi) Talmon and Dr. Naama Koifman for their valuable assistance and discussions.

Appendix A. Supplementary material

Supplementary data to this article can be found online at https://doi.org/10.1016/j.jcis.2020.02.048.

References

[1] N. Astrini, L. Anah, A. Haryono, Crosslinking Parameter on the preparation of cellulose based hydrogel with divynilsulfone, Procedia Chem. 4 (2012) 275–281.
[2] X. Shen, J.L. Shamshina, P. Berton, G. Gurau, R.D. Rogers, Hydrogels based on cellulose and chitin: fabrication, properties, and applications, Green Chem. 18 (1) (2015) 53–75.
[3] N. Quennouz, S.M. Hashmi, H.S. Choi, J.W. Kim, C.O. Osuji, Rheology of cellulose nanofibrils in the presence of surfactants, Soft Matter 12 (1) (2016) 157–164.
[4] T. Saito, A. Isogai, TEMPO-mediated oxidation of native cellulose. The effect of oxidation conditions on chemical and crystal structures of the water-insoluble fractions, Biomacromolecules 5 (5) (2004) 1983.
[5] E. Abraham, B. Deepa, L. Pothan, M. Jacob, S. Thomas, U. Cvelbar, R. Anandjiwala, Extraction of nanocellulose fibrils from lignocellulosic fibres: A novel approach, Carbohydr. Polym. 86 (4) (2011) 1468–1475.
[6] A. Sannino, C. Demitri, M. Madaghiele, Biodegradable cellulose-based hydrogels: design and applications, Materials 2 (2) (2009) 353–373.
[7] M.N. Alam, L. Christopher, Natural cellulose-chitosan crosslinked superabsorbent hydrogels with superior swelling properties, ACS Sustainable Chem. Eng. 6 (7) (2018) 8736–8742.
[8] N. Reddy, Y. Yang, Citric acid cross-linking of starch films, Food Chem. 118 (3) (2010) 702–711.
[9] N.S. Capanema, A.A. Mansur, A.C. de Jesus, S.M. Carvalho, L.C. de Oliveira, H.S. Mansur, Superabsorbent crosslinked carboxymethyl cellulose-PEG hydrogels for potential wound dressing applications, Int. J. Biol. Macromol. 106 (2018) 1218–1234.
[10] M.N. Alam, M.S. Islam, L.P. Christopher, Sustainable production of cellulose-based hydrogels with superb absorbing potential in physiological saline, ACS Omega 4 (5) (2019) 9419–9426.
[11] F. Zhao, E. Repo, Y. Song, D. Yin, S.B. Hammouda, L. Chen, S. Kalliola, J. Tang, K.C. Tam, M. Sillanpää, Polyethylenimine-cross-linked cellulose nanocrystals for highly efficient recovery of rare earth elements from water and a mechanism study, Green Chem. 19 (20) (2017) 4816–4828.
[12] O. Boussif, F. Lezoualc'h, M.A. Zanta, M.D. Mergny, D. Scherman, B. Demeneix, J.-P. Behr, A versatile vector for gene and oligonucleotide transfer into cells in culture and in vivo: polyethylenimine, Proc. Natl. Acad. Sci. 92 (16) (1995) 7297–7301.

[13] U. Lungwitz, M. Breunig, T. Blunk, A. Göpferich, Polyethylenimine-based non-viral gene delivery systems, Eur. J. Pharm. Biopharm. 60 (2) (2005) 247–266.
[14] N. Lavoine, L. Bergström, Nanocellulose-based foams and aerogels: processing, properties, and applications, J. Mater. Chem. A 5 (31) (2017) 16105–16117.
[15] C. Antonini, T. Wu, T. Zimmermann, A. Kherbeche, M.-J. Thoraval, G. Nyström, T. Geiger, Ultra-porous nanocellulose foams: A facile and scalable fabrication approach, Nanomaterials 9 (8) (2019) 1142.
[16] S. Trombino, R. Cassano, E. Bloise, R. Muzzalupo, L. Tavano, N. Picci, Synthesis and antioxidant activity evaluation of a novel cellulose hydrogel containing trans-ferulic acid, Carbohydr. Polym. 75 (1) (2009) 184–188.
[17] O.M. Jensen, Water absorption of superabsorbent polymers in a cementitious environment, in: International RILEM Conference on Advances in Construction Materials Through Science and Engineering, RILEM Publications SARL, 2011, pp. 22–35.
[18] G. Kowalski, K. Kijowska, M. Witczak, Ł. Kuterasiński, M. Łukasiewicz, Synthesis and effect of structure on swelling properties of hydrogels based on high methylated pectin and acrylic polymers, Polymers 11 (1) (2019) 114.
[19] V.S. Raghuwanshi, G. Garnier, Characterisation of hydrogels: Linking the nano to the microscale, Adv. Colloid Interface Sci. 274 (2019) 102044.
[20] J. Liu, C. Zhang, D. Miao, S. Sui, F. Deng, C. Dong, L. Zhang, P. Zhu, Preparation and characterization of carboxymethylcellulose hydrogel fibers, J. Eng. Fibers Fabrics 13 (3) (2018). 155892501801300302.
[21] L. Mendoza, W. Batchelor, R.F. Tabor, G. Garnier, Gelation mechanism of cellulose nanofibre gels: A colloids and interfacial perspective, J. Colloid Interface Sci. 509 (2018) 39–46.
[22] Y. Mao, K. Liu, C. Zhan, L. Geng, B. Chu, B.S. Hsiao, Characterization of nanocellulose using small-angle neutron, X-ray, and dynamic light scattering techniques, J. Phys. Chem. B 121 (6) (2017) 1340–1351.
[23] J. Schmitt, V. Calabrese, M.A. Da Silva, S. Lindhoud, V. Alfredsson, J.L. Scott, K.J. Edler, TEMPO-oxidised cellulose nanofibrils; probing the mechanisms of gelation via small angle X-ray scattering, PCCP 20 (23) (2018) 16012–16020.
[24] S. Koizumi, Y. Tomita, T. Kondo, T. Hashimoto, What factors determine hierarchical structure of microbial cellulose-interplay among physics, chemistry and biology, in: Macromolecular symposia, Wiley Online Library, 2009, pp. 110–118.
[25] T. Saito, S. Kimura, Y. Nishiyama, A. Isogai, Cellulose nanofibers prepared by TEMPO-mediated oxidation of native cellulose, Biomacromolecules 8 (8) (2007) 2485.
[26] D. da Silva Perez, S. Montanari, M.R. Vignon, TEMPO-mediated oxidation of cellulose III, Biomacromolecules 4 (5) (2003) 1417–1425.
[27] L. Mendoza, L. Hossain, E. Downey, C. Scales, W. Batchelor, G. Garnier, Carboxylated nanocellulose foams as superabsorbents, J. Colloid Interface Sci. 538 (2019) 433–439.
[28] L. Issman, Y. Talmon, Cryo-SEM specimen preparation under controlled temperature and concentration conditions, J. Microsc. 246 (1) (2012) 60–69.
[29] N.M. Kirby, S.T. Mudie, A.M. Hawley, D.J. Cookson, H.D. Mertens, N. Cowieson, V. Samardzic-Boban, A low-background-intensity focusing small-angle X-ray scattering undulator beamline, J. Appl. Crystallogr. 46 (6) (2013) 1670–1680.
[30] O. Glatter, O. Kratky, Small Angle X-ray Scattering., Academic press., 1982.
[31] V.S. Raghuwanshi, M. Ochmann, A. Hoell, F. Polzer, K. Rademann, Deep eutectic solvents for the self-assembly of gold nanoparticles: a SAXS, UV–Vis, and TEM investigation, Langmuir 30 (21) (2014) 6038–6046.
[32] A.M. Castilla, E.R. Draper, M.C. Nolan, C. Brasnett, A. Seddon, L.L. Mears, N. Cowieson, D.J. Adams, Self-sorted oligophenylvinylene and perylene bisimide hydrogels, Sci. Rep. 7 (1) (2017) 8380.
[33] E. Anitas, Fractal fragmentation and small-angle scattering, in: Journal of Physics: Conference Series, IOP Publishing. 633(1) (2015) 012119.
[34] M. Shibayama, Small angle neutron scattering on gels, Soft Matter Charact. (2008) 783–832.
[35] J.C. Courtenay, S.M. Ramalhete, W.J. Skuze, R. Soni, Y.Z. Khimyak, K.J. Edler, J.L. Scott, Unravelling cationic cellulose nanofibril hydrogel structure: NMR spectroscopy and small angle neutron scattering analyses, Soft Matter 14 (2) (2018) 255–263.
[36] A.R. Klotz, DNA Polymer Physics in Complex Nanofluidic Environments. PhD thesis (McGill University, Montreal, Quebec), 2015.
[37] J. Gao, J. Liu, H. Peng, Y. Wang, S. Cheng, Z. Lei, Preparation of a low-cost and eco-friendly superabsorbent composite based on wheat bran and laterite for potential application in Chinese herbal medicine growth, R. Soc. Open Sci. 5 (5) (2018) 180007.
[38] M.I. Voronova, A.G. Zakharov, O.Y. Kuznetsov, O.V. Surov, The effect of drying technique of nanocellulose dispersions on properties of dried materials, Mater. Lett. 68 (2012) 164–167.
[39] L. Salmén, J.S. Stevanic, Effect of drying conditions on cellulose microfibril aggregation and "hornification", Cellulose 25 (11) (2018) 6333–6344.
[40] O. Nechyporchuk, M.N. Belgacem, F. Pignon, Concentration effect of TEMPO-oxidized nanofibrillated cellulose aqueous suspensions on the flow instabilities and small-angle X-ray scattering structural characterization, Cellulose 22 (4) (2015) 2197–2210.